A series multi-step approach for operation Co-optimization of integrated power and natural gas systems

Faridpak, Behdad; Farrokhifar, Meisam; Murzakhanov, Ilgiz; Safari, Amin

Published in:
Energy

DOI:
10.1016/j.energy.2020.117897

Publication date:
2020

Energy 204 (2020) 117897

Contents lists available at ScienceDirect

Energy

journal homepage: www.elsevier.com/locate/energy

A series multi-step approach for operation Co-optimization of integrated power and natural gas systems

Behdad Faridpak [a], Meisam Farrokhifar, Ph.D. [b, c, *], Ilgiz Murzakhanov [d], Amin Safari, Ph.D. [e]

[a] Faculty of Electrical and Computer Engineering, University of Tabriz, Tabriz, Iran
[b] Center for Energy Systems, Skolkovo Institute of Science and Technology (Skoltech), Moscow, Russia
[c] Faculty of Science and Engineering, University of Groningen, Groningen, the Netherlands
[d] Department of Electrical Engineering, Technical University of Denmark, Kgs.Lyngby, Denmark
[e] Department of Electrical Engineering, Azarbaijan Shahid Madani University, Tabriz, Iran

ARTICLE INFO

Article history:
Received 26 August 2019
Received in revised form
4 May 2020
Accepted 16 May 2020
Available online 1 June 2020

Keywords:
Optimal operation
Uncertainty
Integrated power system and natural gas network
Lagrange relaxation
Risk analysis

ABSTRACT

Power to gas units and gas turbines have provided considerable opportunities for bidirectional interdependency between electric power and natural gas infrastructures. This paper proposes a series of multi-step strategy with surrogate Lagrange relaxation for operation co-optimization of an integrated power and natural gas system. At first, the value of coordination capacity is considered as a contract to avoid dysfunction in each system. Then, the uncertainties and risks analysis associated with wind speed, solar radiation, and load fluctuation are implemented by generating stochastic scenarios. Finally, before employing surrogate Lagrange relaxation, the non-linear and non-convex gas flow constraint is linearized by two-dimension piecewise linearization. In the proposed procedure, constraints for energy storages and renewable energy sources are included. Two case studies are employed to verify the effectiveness of the proposed method. The surrogate Lagrange relaxation approach with coordination branch & cut method enhances the accuracy of convergence and can effectively reduce the decision-making time.

1. Introduction

The reforming of energy systems in some societies has increased the interest in coordinating between the separate primary energy and electricity infrastructures [1]. The impact of interconnection between electricity and other energy systems such as hydrogen, heat and natural gas (NG) was analyzed in recent years. Hybrid electric vehicles can benefit from the integration of hydrogen and electricity networks [2]. The combination of electricity and heat systems results in power and heat purchase saving [3]. The joint operation of NG and power networks could reduce investment and operation costs [4]. There are different aims in optimization problems related to electricity and energy systems. In this context, an optimization framework was proposed based on an evolutionary algorithm for improving the reliability of the system [5]. The authors in Ref. [6] addressed an energy model to increase the share of renewable energy sources (RESs). In Ref. [7], variable behavior of loads and energy cost curves were considered for loss reduction. Also, the authors in Ref. [4] minimized co-planning costs in an interconnected power and NG system. Among all types of primary energy systems, the NG network has proper interdependency specifications [8]. From this point of view, employing an integrated approach offers solutions to overcome some of the energy concerns such as environmental damage associated with the use of fossil fuels, power shortage, economic issues [1]. However, operation co-optimization of the integrated power and gas system (IPGS) is challenging due to the following reasons. Firstly, the conventional operating principles of individual systems need restoration. Secondly, security risk concerns emerge for interconnecting between them. Thirdly, the operation and scheduling of the integrated system under the stochastic framework with incorporating uncertain RESs nature and load demand have their own complexities [9].

The operation co-optimization of IPGS is a difficult task due to a large number of variables and parameters affect this procedure. In

* Corresponding author. Center for Energy Science and Technology, Skolkovo Institute of Science and Technology, Moscow, Russia.
E-mail address: m.farrokhi@skoltech.ru (M. Farrokhifar).

https://doi.org/10.1016/j.energy.2020.117897
0360-5442/

Nomenclature

Constants & parameter

$C_p(t)$	Energy price [$/MWh]
$C_g(t)$	Gas price [$/MWh]
x	Line reactance [Ω]
$VOLL$	Penalty for load shedding [$]
C_{SU}/C_{SD}	Start-up/shut-down cost of generator [$]
RU/RD	Ramp up/down rate of generator [MW]
SU/SD	Start-up/shut-down rate of generator [MW]
Γ_c	Compressor factor
u_{r1}/u_{r2}	Autoregressive/moving parameters
ξ_{CVaR}	CVaR with confident level α
ξ_α	Auxiliary variables for calculating CVaR
$Y(t)$	Standard location of estimated point
$e(t)$	Estimated point of each χ
$\lambda(t)$	Lagrange multipliers
$LP(t)$	Load profile
τ	Normal white noise process
$y(t)$	Time series value
$\upsilon_{ci}(t)/\upsilon_{co}(t)/\upsilon_{rate}(t)$	Cut in/cut out/nominal wind speed [m/s]
$\varrho\Lambda$	Beta PDF parameters
k_V	Voltage temperature coefficient [V/°C]
k_C	Current temperature coefficient [V/°C]
V_{OC}/V_{MPP}	Open circuit/MPPT voltage [V]
I_{SC}/I_{MPP}	Short circuit/MPPT currents [A]
FF	Fill factor
N_{ot}/T_a	Nominal/ambient temperature [V/°C]
ψ	Coefficient of electricity-gas conversion
φ	Coefficient of gas-electricity conversion
η	Efficiency
T	Total operation time which equals to 24 h
p_ε	Probability of scenarios
α	Confident level
β	Risk factor
D	Pipeline diameter [m]
Δx	Pipe length [m]
F	Pipe friction factor
R	Specific gas constant [$m^3 bar/kg^\circ C$]
Z	Compressibility factor
ρ_0	Gas density in standard conditions [$kg/\ m^3$]
$\mu(t)$	Mean value
σ	Standard deviation
$G_d(t)$	Natural gas load [MWh]
$r_{sk}(t)$	Skewness of estimated points
$r_{ku}(t)$	Kurtosis of estimated points
N_{kl}	Total number of linear segments
γ	ESs penetration

Indices

i,j	Subscript indices of buses in power systems
k,l	Subscript indices of nodes in natural gas networks
min	Superscript indication of minimum value
max	Superscript indication of maximum value
ε	Subscript indices of scenarios
$\rho\upsilon/wt/\rho$	Subscript indices of PVs/WTs/ESs
$w/tg/gt/b$	Subscript indices of wells/TGs/GTs/P2Gs
$\Im$	Subscript indices of linear segment

Sets

Ω_T	Set of operation time intervals
Ω_P	Set of all generators
Ω_W	Set of wells
Ω_{TG}	Set of thermal generators
Ω_{GT}	Set of gas turbines
Ω_{PV}	Set of photo-voltaic modules
Ω_{WT}	Set of wind turbine unites
Ω_{ES}	Set of energy storage systems
Ω_B	Set of power to gas units
Ω_χ	Set of uncertainty variables
Ω_E	Set of scenarios
Ω_{R1}/Ω_{R2}	Set of autoregressive/moving parameters

Variables

$TOC(t)$	Total operating cost of integrated systems [$]
$PSC(t)$	Operating cost of power system [$]
$GNC(t)$	Operating cost of natural gas network [$]
$LSC(t)$	Load shedding cost [$]
$P(t)$	Output power of generator [MW]
$P_{ij}(t)$	Transmitted power between buses i and j [MW]
$P_{PV}(t)$	Output power of PV [MW]
$P_{WT}(t)$	Output power of WT [MW]
$P_d(t)$	Electrical load [MW]
$G(t)$	Extracted gas from well [MWh]
$L_{sh}(t)$	Load shedding [MW]
$SUC(t)/SDC(t)$	Start-up/shut-down cost of generator at time t [$]
$P_{ch}(t)/P_{dch}(t)$	Charge/discharge power of ES [MW]
$SOC(t)$	State of charge
$\delta(t)$	Voltage angle [rad]
$\pi(t)$	Node pressure of natural gas network [bar]
$\Theta(t)$	Square of nodal pressure [bar]
$\tilde{q}(t)/q^{in}(t)/q^{out}(t)$	Average/inlet/outlet Gas flow in pipeline [Mm^3]
$\upsilon(t)$	Wind speed [m/s]
$s(t)$	Solar radiation [kW/m^2]
$\partial_{GT}(t)/\partial_{P2G}(t)$	Adjustment power value [MW]
$I_{SU}(t)$	Start-up state (1 if power generator is starting-up otherwise is 0) [binary]
$I_{SD}(t)$	Shut-down state (1 if power generator is shutting-down otherwise is 0) [binary]
$I_S(t)$	on/off status (1 if power generator is on otherwise is 0) [binary]

addition, large dimensions and complex equations disrupt temporal decisions. Several studies have considered the optimal operation of IPGS. In Refs. [10], an electricity grid was integrated with an NG network via the installation of gas turbines (GTs). Also, the authors tried to achieve optimized scheduling of multi-region gas and power complementary system considering tiered NG tariff. In Ref. [11], an optimal scheduling model for integrated energy systems considering the dynamic characteristics and uncertainty of wind power is proposed to improve the economy and security of integrated energy systems. Co-optimization scheduling of interdependent power and NG systems with electricity and gas uncertainties was performed in Ref. [12]. The authors in Ref. [4] presented a multi-stage contingency-constrained co-planning for electricity-gas systems interconnected with GTs and power to gas (P2G) plants using iterative Benders decomposition. This model considers the long-term co-planning for electricity-gas systems

with the short-term operation constraints and N-1 reliability criterion, which is formulated as a mixed-integer linear programming (MILP) problem. By convex decoupled-synergetic strategies in Ref. [13], an attempt was made to solve the robust multi-objective power and NG flow problem considering P2G. As well, a similar MILP-based approach was applied in Ref. [14] to achieve the optimal power flow of IPGS. In Refs. [15], security modeling of the IPGS by analyzing critical situations and potentials for performance optimization was analyzed. Accordingly, the purpose of security modeling is to show, through quantification of impacts of the IPGS, that the failures of the radial NG subsystem, in terms of security, as a rule, are more critical for the IPGS in the electric power subsystem. To minimize the TOC, the authors in Ref. [16] provided an analysis of the pricing and control of the market. Also, data-driven distributionally robust optimization [17] and game theory [18] are among the optimization methods applied to the optimal co-operation problem.

Given the background perspective, an operation co-optimization method is developed for an IPGS in this paper. In this regard, a comprehensive series multi-step approach is presented. Firstly, the conventional non-convex MINLP operation co-optimization problem of IPGS is solved to determine contract value for power exchange. Secondly, with the approximate non-linearity approach, the stochastic operation of IPGS is optimized with incorporating risk analysis in which uncertainty variables cause a scenario-based analysis. To discuss uncertainties and to associate risk analysis, the scenarios were generated by 2m + 1 point estimated method (PEM) [19]. The conditional value-at-risk (CVaR) is employed to analyze the financial risk of IPGS. Correspondingly, the initial values of the Lagrange multiplier and worst-scenario are determined. Finally, the proposed problem is reformed into a MILP problem by utilizing piecewise linearization. In addition, the obtained complex and large-scale MILP problem is decomposed to sub-problems (SPs) by the duality theory and surrogate Lagrangian relaxation (SLR). The decomposed and separate sub-problems are solved by utilizing branch and cut (B&C) method. The coordination of SPs is achieved with updating Lagrange multipliers after solving the SPs subject to surrogate optimality condition.

For the first time, our paper proposes a series multi-step approach in optimal co-operating of IPGS. Our approach is a comprehensive solution that includes a modified form of risk analysis, uncertainties, linearization, and relaxation. While previous researches were applied just one or two of those in the systems integration area. Also, incorporating the risk analysis for minimizing operation costs and applying SLR as a relaxation method to accelerate the optimization process are among the main advantages of the proposed method.

This paper is organized as follows. The mathematical model is presented after the introduction section. Then, the uncertainty variables are addressed in the third section. The proposed series multi-step approach is presented in section 4. The numerical results are analyzed in section 5. The conclusion is the last section of this paper.

2. Mathematical model of the operation Co-optimization problem

In this section, the mathematical model for the operation co-optimization of an IPGS is presented. There are several approaches to minimize the risk caused by uncertainty. A few of the most famous approaches are stochastic programming, robust optimization, chance-constrained programming, and distributionally robust optimization. Stochastic programming minimizes total expected cost, while robust optimization minimizes system cost for the worst-case scenario. As a result, the result of the robust optimization is optimal for the worst case and is feasible for all other outcomes. It can be concluded that stochastic programming in expectation has a lower cost than robust optimization, but has a higher cost in the worst-case scenario. The robust optimization algorithm can be further advanced to the adaptive robust optimization algorithm by checking vertices of the worst-case scenarios. In the chance-constrained programming, the violation of each constraint is allowed by some tolerance value, as a result allowing greater total violation. Finally, in distributionally robust optimization, no assumption on the probability distribution of the uncertainty is made, but rather an ambiguity set is constructed. In the current work, the CVaR metric was used to incorporate uncertainty. The main objective function of the proposed stochastic problem is minimizing expected total operation cost (TOC) over the chosen set of scenarios, as stated in (1). In order to consider the influence of risk caused by uncertainty in the optimization problem, the CVaR metric is utilized. CVaR displays the system cost in the case of the worst scenario realization.

EQUATION SET 1 Objective Function

$$TOC = \sum_{\varepsilon} p_{\varepsilon}.[PSC + GNC + LSC] \qquad \forall \varepsilon \in \Omega_E \tag{1a}$$

$$PSC = \sum_{t}\sum_{p}\left[C_p(t).P_p(t) + SUC_p(t) + SDC_p(t)\right] \quad \forall t \in \Omega_T, \forall p \in \Omega_P \tag{1b}$$

$$GNC = \sum_{t}\sum_{w} C_g(t).G_w(t) \qquad \forall t \in \Omega_T, \forall w \in \Omega_W \tag{1c}$$

$$LSC = VOLL.\sum_{t}\sum_{i} L^{i}_{sh}(t) \qquad \forall t \in \Omega_T \tag{1d}$$

TOC contains three parts as demonstrated in (1a). In (1b), PSC shows the operating cost of the power system and consists of power generation and start-up/shut-down costs. According to (1c), the operating cost of the NG network (GNC) equals to the cost of extracting NG from gas wells. Also, load shedding cost (LSC) for each bus includes a penalty factor that is modeled by a large coefficient (VOLL) in (1d). In fact, LSC is the cost of unsupplied loads due to the shortage of resources.

It should be noted that in our problem, power generation from renewable and non-renewable sources are considered. Accordingly, thermal generators (TGs) and gas turbines (GTs) are categorized as generators fed from non-renewable sources. The number of these generators (Ω_P) is equal to the summation of GTs (Ω_{GT}) and TGs (Ω_{TG}) numbers.

EQUATION SET 2 Power System

$$P_p(t) = P_{tg}(t) + P_{gt}(t) \quad \forall t \in \Omega_T, \forall p \in \Omega_P, \forall tg \in \Omega_{TG}, \forall gt \in \Omega_{GT} \tag{2a}$$

$$P_{ij}(t) = \left(\delta_i(t) - \delta_j(t)\right) / x_{ij} \qquad \forall t \in \Omega_T \tag{2b}$$

$$-P^{max}_{ij} \le P_{ij}(t) \le P^{max}_{ij} \qquad \forall t \in \Omega_T \tag{2c}$$

$$P^{min}_{tg}.I_{S,p}(t) \le P_{tg}(t) \le P^{max}_{tg}.I_{S,p}(t) \qquad \forall t \in \Omega_T, \forall tg \in \Omega_{tg} \tag{2d}$$

$$SUC_p(t) = I_{SU,p}(t).C_{SU} \qquad \forall t \in \Omega_T, \forall p \in \Omega_P \tag{2e}$$

$$SDC_p(t) = I_{SD,p}(t).C_{SD} \qquad \forall t \in \Omega_T, \forall p \in \Omega_P \tag{2f}$$

$$I_{SU,p}(t) - I_{SD,p}(t) = I_{S,p}(t) - I_{S,p}(t) \qquad \forall t \in \Omega_T, \forall p \in \Omega_P \tag{2g}$$

$$P_p(t) - P_p(t-1) \le RU_p \qquad \forall t \in \Omega_T, \forall p \in \Omega_{TG} \tag{2h}$$

$$P_p(t-1) - P_p(t) \le RD_p \qquad \forall t \in \Omega_T, \forall p \in \Omega_P \tag{2i}$$

$$L^i_{sh}(t) \le P^i_d(t) \qquad \forall t \in \Omega_T \tag{2j}$$

$$0 \le P_{WT,wt}(t) \le P^{max}_{WT,wt} \qquad \forall t \in \Omega_T, \forall wt \in \Omega_{WT} \tag{2k}$$

$$0 \le P_{PV,\rho v}(t) \le P^{max}_{PV,\rho v} \qquad \forall t \in \Omega_T, \forall \rho v \in \Omega_{PV} \tag{2l}$$

$$SOC_\rho(t+1) = SOC_\rho(t) + \left[P_{ch,\rho}(t).\eta_{ch} - P_{dch,\rho}(t) \,/\, \eta_{dch}\right] \qquad \forall t \in \Omega_T, \forall \rho \in \Omega_{ES} \tag{2m}$$

$$0 \le P_{ch,\rho}(t) \le I_{ch,\rho}(t).P^{max}_{ch,\rho} \qquad \forall t \in \Omega_T, \forall \rho \in \Omega_{ES} \tag{2n}$$

$$0 \le P_{dch,\rho}(t) \le I_{dch,\rho}(t).P^{max}_{dch,\rho} \qquad \forall t \in \Omega_T, \forall \rho \in \Omega_{ES} \tag{2o}$$

$$I_{ch,\rho}(t) + I_{dch,\rho}(t) \le 1 \qquad \forall t \in \Omega_T, \forall \rho \in \Omega_{ES} \tag{2p}$$

$$SOC^{min}_\rho \le SOC_\rho(t) \le SOC^{max}_\rho \qquad \forall t \in \Omega_T, \forall \rho \in \Omega_{ES} \tag{2q}$$

$$DOD_\rho = DOD_\rho(Initial) \qquad \forall \rho \in \Omega_{ES} \tag{2r}$$

$$SOC_\rho(1) = SOC_\rho(24) \qquad \forall \rho \in \Omega_{ES} \tag{2s}$$

Constraints of the optimization problem are divided into three main parts: a) Power system (2), b) NG network (2), c) Power and NG networks integration (3) described in the following.

Generated power from non-renewable sources includes generated power from TGs and GTs are modeled in (2a). It is worth mentioning that, DC power flow method was applied in this paper for the suited power system. According to (2b), transmitted power between two buses is calculated by the ratio of their voltage angle difference over the reactance of lines in between. Also, the line capacity bounds for the transmitted power are shown in (2c). Technical power range of each TG is indicated in (2d). In (2e) and (2f), the costs of start-up or shut-down of generators are modeled. Regarding the generators on/of status, (2g) shows that generators are required to operate in either the start-up, shut-down, or normal conditions [20]. This constraint can be applied via defining two binary variables. In addition, (2h) and (2i) show the ramp up and ramp down limits of power generators at different times. In order to control load shedding, (2j) sets a limitation for this issue. Accordingly, the maximum amount of L_{sh} in each bus equals to the amount of load in that bus. As well, (2k) and (2l) indicate a range on the amounts of the generated power from wind turbine (WT) and photo-voltaic (PV), respectively. In (2m)-(2s), the constraints of the storage system are presented [21]. In this regard, (2m) determines the amount of stored energy. Constraints of charge and discharge power are shown as (2n) and (2o). Furthermore, (2p) shows that ESs are required to operate in either the charging or discharging conditions. In addition, (2q) determines the minimum and maximum *SOC*. The predefined values for the depth of discharge (DOD) are determined in (2r). Also, (2s) demonstrates that stored energy in ES at the beginning and the end of the optimization period should be equal [22].

EQUATION SET 3 Natural Gas Network

$$\tilde{q}_{kl}(t) = C_{kl}.sign(\pi_k(t), \pi_l(t)).\sqrt{\pi_k(t)^2 - \pi_l(t)^2} \qquad \forall t \in \Omega_T \tag{3a}$$

$$C_{kl} = \left(\frac{\pi}{4}\right)\frac{D^5_{kl}}{\Delta x_{kl} F_{kl} R T_g Z \rho^2_0} \tag{3b}$$

$$sign(\pi_k(t), \pi_l(t)) = \begin{cases} 1, & \pi_k(t) \ge \pi_l(t) \\ -1, & \pi_k(t) < \pi_l(t) \end{cases} \qquad \forall t \in \Omega_T \tag{3c}$$

$$\tilde{q}_{kl}(t) = \frac{q^{in}_{kl}(t) + q^{out}_{kl}(t)}{2} \qquad \forall t \in \Omega_T \tag{3d}$$

$$\pi_k(t) \le \Gamma_c \pi_l(t) \qquad \forall t \in \Omega_T \tag{3e}$$

$$\pi^{min}_k \le \pi_k(t) \le \pi^{max}_k \qquad \forall t \in \Omega_T \tag{3f}$$

$$G^{min}_w \le G_w(t) \le G^{max}_w \qquad \forall t \in \Omega_T, \forall w \in \Omega_W \tag{3g}$$

The mathematical model of NG distribution network is presented by (3). In these equations, the average input and output pressure, as well as constraints of gas pressure in each node and the operating capacity of the compressors, are expressed.

EQUATION SET 4 Integration of Power System and Natural Gas Network

$$G_{P2G,b}(t) = \psi.P_{P2G,b}(t).\eta_{P2G} \qquad \forall t \in \Omega_T, b \in \Omega_B \tag{4a}$$

$$P_{GT,gt}(t) = \phi.G_{GT,gt}(t).\eta_{GT} \qquad \forall t \in \Omega_T, gt \in \Omega_{GT} \tag{4b}$$

$$P^{\min}_{P2G,b}.\Delta t \le P_{P2G,b}(t) \le P^{\max}_{P2G,b}.\Delta t \qquad \forall t \in \Omega_T, b \in \Omega_B \tag{4c}$$

$$P^{\min}_{GT,gt}.\Delta t \le P_{GT,gt}(t) \le P^{\max}_{GT,gt}.\Delta t \qquad \forall t \in \Omega_T, gt \in \Omega_{GT} \tag{4d}$$

$$\sum_{gt} P_G(t) + \sum_{tg} P_T(t) + \sum_{\rho v} P_{PV}(t) + \sum_{wt} P_{WT}(t) + \sum_{\rho} P_{dch}(t) = \sum_{b} P_{P2G}(t) + \sum_{i} P_d(t) + \sum_{\rho} P_{ch}(t) + \sum_{i} l_{sh}(t)$$
$$\forall t \in \Omega_T, \forall gt \in \Omega_{GT}, \forall tg \in \Omega_{TG}, \forall \rho v \in \Omega_{PV}, \forall wt \in \Omega_{WT}, \forall \rho \in \Omega_{ES}, \forall b \in \Omega_B \tag{4e}$$

$$\sum_{w} G_w(t) + \sum_{b} G_{P2G}(t) = \sum_{gt} G_{GT}(t) + \sum_{k} G_d(t)$$
$$\forall t \in \Omega_T, \forall b \in \Omega_B, \forall gt \in \Omega_{GT}, \forall w \in \Omega_W \tag{4f}$$

By providing separate models for the power system and NG network, there is a need for interconnecting these two types of energy. To achieve a bidirectional energy conversion P2G system, which converts electric power into gas, and GT, which converts NG into electrical power, are utilized. The P2Gs consume low-price electrical power or excess generated power from RESs to sell energy to the NG network [23]. Besides, GTs are operated as backups at the high-price time intervals of electric energy to decrease pressure on the TGs. Generated gas by P2G unit is calculated according to (4a). On the contrary, the generated power of each GT is related to received gas and gas to electricity conversion ratio, as modeled in (4b). The operation constraints of joint units GTs and

P2Gs are presented in (4c) and (4d), respectively. In (4e), the power balance has been modeled for IPGS. With a similar relation, the mathematical model of gas balancing is presented in (4f). It must be noted that P2G unit is considered as a consumer for the power system and as a generator for the NG network. However, GT has a vice versa duty.

3. Mathematical model of uncertainty variables

Due to the presence of the RESs and fluctuations of load, the optimization problem of the IPGS consists of uncertainty variables. Accordingly, uncertainty variables of the proposed problem include $\upsilon(t)$, $s(t)$ and $LP(t)$. These variables are modeled according to a two-stage stochastic framework, which is explained further.

EQUATION SET 5 Uncertainty Variables

$$y(t)=\sum_{r1}u_{r1}y(t-r)+\tau(t)-\sum_{r2}u_{r2}\tau(t-r) \quad \forall t\in\Omega_T,\ \forall r1\in\Omega_{R1},\ \forall r2\in\Omega_{R2} \tag{5a}$$

$$\upsilon_{wt}(t)=\mu_{wt}(t)+\sigma_{wt}.y(t) \qquad \forall t\in\Omega_T,\ \forall wt\in\Omega_{WT} \tag{5b}$$

$$P_{WT,wt}(t)=\begin{cases}0 & 0\le\upsilon(t)\le\upsilon_{ci}\ or\ \upsilon(t)\ge\upsilon_{co}\\ \dfrac{P_{rat}(\upsilon_{wt}(t)-\upsilon_{ci})}{(\upsilon_{rat}-\upsilon_{ci})} & \upsilon_{ci}\le\upsilon(t)\le\upsilon_{rat}\\ P_{rat} & \upsilon_{rat}\le\upsilon(t)\le\upsilon_{co}\end{cases} \quad \forall t\in\Omega_T,\ \forall wt\in\Omega_{WT} \tag{5c}$$

$$f(s_{\rho v})=\begin{cases}\dfrac{\Gamma(\varrho_{\rho v}+\Lambda_{\rho v})}{\Gamma(\varrho_{\rho v})\Gamma(\Lambda_{\rho v})}.s_{\rho v}(t)^{(\varrho_{\rho v}-1)}.\left(1-s_{\rho v}(t)\right)^{(\Lambda_{\rho v}-1)},\\ 0\le s_{\rho v}(t)\le 1\\ 0,\\ \text{Otherwise}\end{cases} \quad \forall t\in\Omega_T,\ \forall \rho v\in\Omega_{PV} \tag{5d}$$

$$P_{PV,\rho v}(t)=FF_{\rho v}.V_{\rho v}(t).I_{\rho v}(t) \qquad \forall t\in\Omega_T,\ \forall \rho v\in\Omega_{PV} \tag{5e}$$

$$I_{\rho v}(t)=s_{\rho v}(t).\left[I_{SC,\rho v}+k_{C,\rho v}\left(T_{C,\rho v}(t)-25\right)\right] \quad \forall t\in\Omega_T,\ \forall \rho v\in\Omega_{PV} \tag{5f}$$

$$V_{\rho v}(t)=V_{OC,\rho v}+k_{V,\rho v}.T_{C,\rho v}(t) \qquad \forall t\in\Omega_T,\ \forall \rho v\in\Omega_{PV} \tag{5g}$$

$$T_{C,\rho v}(t)=T_{a,\rho v}+s_{\rho v}(t).\frac{N_{ot,\rho v}(t)-20}{0.8} \quad \forall t\in\Omega_T,\ \forall \rho v\in\Omega_{PV} \tag{5h}$$

$$FF_{\rho v}=\frac{V_{MPP,\rho v}.I_{MPP,\rho v}}{V_{OC,\rho v}.I_{SC,\rho v}} \qquad \forall t\in\Omega_T,\ \forall \rho v\in\Omega_{PV} \tag{5i}$$

$$P_d^i(t)=P_d^{i,max}.LP(t) \qquad \forall t\in\Omega_T \tag{5j}$$

By studying different approaches in order to model uncertainty of wind speed, it is found that the most comprehensive method is auto-regressive moving average (ARMA) time series [24]. The ARMA model is shown in (5a). The stochastic process τ has a normal distribution ($\tau(t)\in\mathcal{N}(0,\sigma^2)$). According to the obtained values for $y(t)$, wind speed scenarios are generated by (5b). Finally, the relation between wind speed and generated power from WT is found by (5c).

The amount of generated power from a PV depends on the amount of the received solar radiation. Based on the results of many papers, particularly [25,26], in order to model the random radiation, the beta probability density function (PDF) has been used as (5d). The stochastic scenarios of generated power from PV are produced by available uncertain values of solar radiation. Furthermore, in (5e)-(5i), calculation of various parameters of the solar panel is presented.

For load uncertainty modeling in each bus, the uniform distribution is used for LP by historical data ($LP(t)\in\mathcal{N}(\mu,\sigma^2)$).

4. Solution methodology

The main objective of the proposed operation co-optimization is to minimize the costs of IPGS by optimizing the operation and scheduling of various components. In this regard, a multi-step methodology is proposed.

Step 1: Coordination capacity.

Originally, the optimization problem of IPGS is an MINLP problem. Also, the contract level can be determined by assuming certain values for input data. So, the amount of exchanged energy between the power system and the NG network can be calculated by solving the proposed problem in a deterministic framework. The amount of exchanged energy in the interconnected node is called coordination capacity (CC). The value of CC is related to the capacity of the joint units (GTs and P2Gs) and considered as a contract between power system and NG network operators over the optimization interval (T). In this regard, the decision variables $\partial_{GT}(t)$ and $\partial_{P2G}(t)$ are defined in (6) to determine the value of CC. Energy exchange between both energy infrastructures may cause dysfunctionality in supplying their loads. Thus, $\partial_{GT}(t)$ and $\partial_{P2G}(t)$ are determined as a contract between the power system and NG network operators and utilized as fixed inputs for other steps of the co-optimization process. For more explanation, the decision variable $\partial_{GT}(t)$ is used to model the transmitted power from the NG network to the electric power system. Inversely, the decision variable $\partial_{P2G}(t)$ is defined to calculate the transmitted power from the electric power system to the NG network. Both $\partial_{GT}(t)$ and $\partial_{P2G}(t)$ determine the coordination capacity of the IPGS. These values are calculated at the beginning of our series multi-step approach for calculating the exchangeable power between power and NG systems as a contract. Accordingly, as stated in (6a) and (6b), the values of $\partial_{GT}(t)$ and $\partial_{P2G}(t)$ are equal to the generated power by GTs and consumed power by P2Gs, respectively. Also, their values are limited by maximum capacity of generated power from GTs and consumed power by P2Gs in (6c) and (6d).

EQUATION SET 6 Determination of Coordination Capacity

$$\partial_{GT}(t)=\sum_{gt}P_{GT,gt}(t) \qquad \forall gt\in\Omega_{GT} \tag{6a}$$

$$\partial_{P2G}(t)=\sum_{b}P_{P2G,b}(t) \qquad \forall b\in\Omega_B \tag{6b}$$

$$0\le\partial_{GT}(t)\le\sum_{gt}P_{GT,gt}^{max} \qquad \forall gt\in\Omega_{GT} \tag{6c}$$

$$0 \le \partial_{P2G}(t) \le \sum_{b} P^{max}_{P2G,b} \qquad \forall b \in \Omega_B \tag{6d}$$

Step 2: Uncertainty characterization.

Regarding the potential of integration by determining CC, the optimal co-scheduling of IPGS should be defined in a stochastic framework. In this regard, different scenarios are produced for uncertain variables such as $\upsilon(t)$, $s(t)$ and $LP(t)$ according to (5). In order to reduce the complexity of the problem and solving time, it is necessary to reduce the number of scenarios into a simpler set with characteristics close to the original scenarios.

Step 2.1: Realization based on 2m + 1 point estimated method.

The 2m + 1 PEM approach is utilized for uncertainty incorporating [19]. Mathematically, the deterministic operation co-optimization of IPGS which is using MINLP method can be expressed as (7a). If a PDF gives random samples $\chi(t) = \{\chi_1(t), \chi_2(t), \ldots, \chi_n(t)\}$, the related points are estimated based on the mean $\mu(t)$ and standard deviation σ of each random variables at any given time by (7b). These samples should retain the statistical information of the original uncertain variable. In this method for each χ the value of m is equal to 1 and the amount of Ω_κ is equal to 3. Therefore, three standard locations and weights are calculated for each variable by (7c) and (7d), respectively. Once all the concentrations $(e_{\chi,\kappa}(t), \omega_{\chi,\kappa})$ are obtained, the function f is evaluated at the points $\{\mu_1(t), \mu_2(t), \ldots, e_\kappa(t), \ldots, \mu_{\Omega_\chi}(t)\}$ yielding $Z_{\chi,\kappa}$, where Z is the vector of output random variables as stated in (7e). Then, by using the weighting factors $\omega_{\chi,\kappa}$ and the $Z_{\chi,\kappa}$ values, the c^{th} raw moment of the output random variables can be estimated according to (7f). The algorithm ends once all the concentrations of all input random variables (wind speed, solar radiation and load demand) are taken into account. Then, the estimated raw moments of the output random variables are used to compute the desired statistical information.

Correspondingly, the values of $\mu(t)$, σ, $r_{sk}(t)$, and $r_{ku}(t)$ are calculated by original scenarios for each uncertain variable. Then, these data are applied to (7). The implementation of the 2m + 1 PEM method is depicted in Fig. 1. According to this schematic, on the base of deterministic values of each χ (Fig. 1a) numerous scenarios are generated using specific PDFs (Fig. 1b). Then, relying on these original scenarios related points are estimated in Fig. 1c.

After applying the 2m + 1 PEM for each χ, the scenarios are generated to the realization of the stochastic framework, according to Fig. 2. In fact, for Ω_χ uncertain variables, Ω_χ stages are needed to generate 3^{Ω_χ} scenarios as final realization scenarios. For simplification, the process in Fig. 2 can be divided into a few two-stage processes in which stage 1 (here-and-now) includes the deterministic amount and stage 2 (wait-and-see) includes three estimated scenarios for each χ.

EQUATION SET 7 Scenario-based Model

$$Z(t) = f(\chi(t)) \tag{7a}$$

$$e_{\chi,\kappa}(t) = \mu_\chi(t) + r_{\chi,\kappa}(t).\sigma_\chi \qquad \forall t \in \Omega_T,\ \forall \chi \in \Omega_\chi,\ \forall \kappa \in \Omega_\kappa \tag{7b}$$

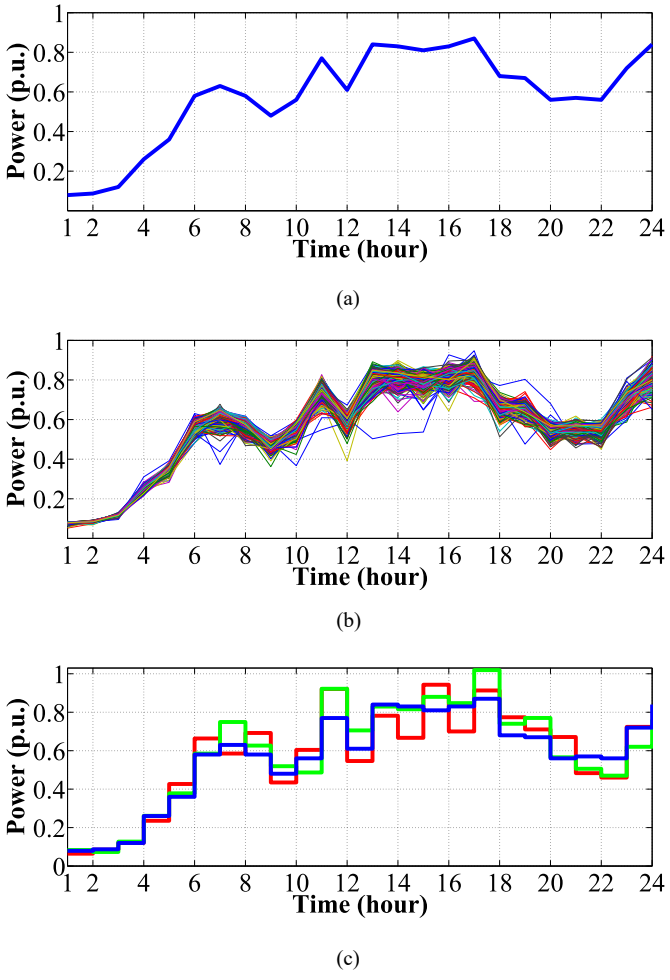

Fig. 1. Illustration of the scenario reduction for an uncertainty variable. a) Deterministic values b) Generating 1000 scenarios under a PDF. c) Production of three scenarios with 2m + 1 PEM.

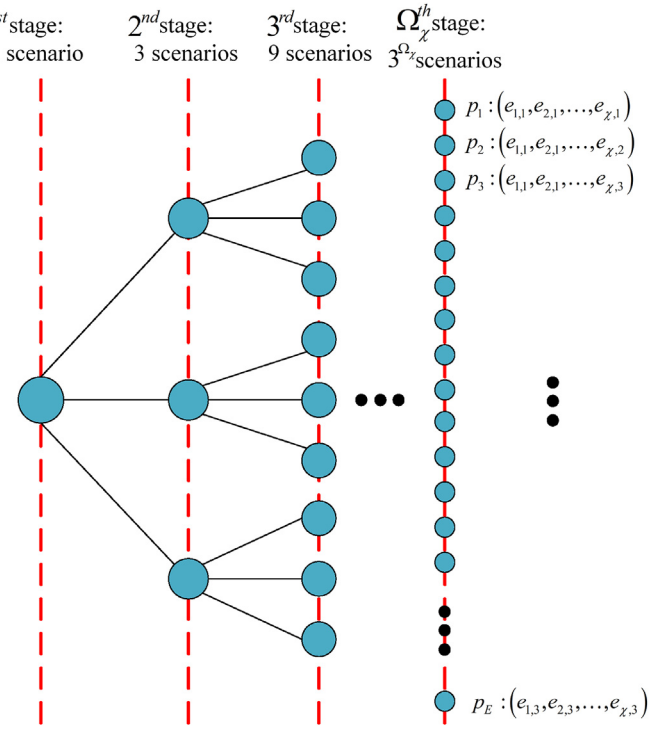

Fig. 2. Scenario tree of Step 2 to stochastic framework modeling.

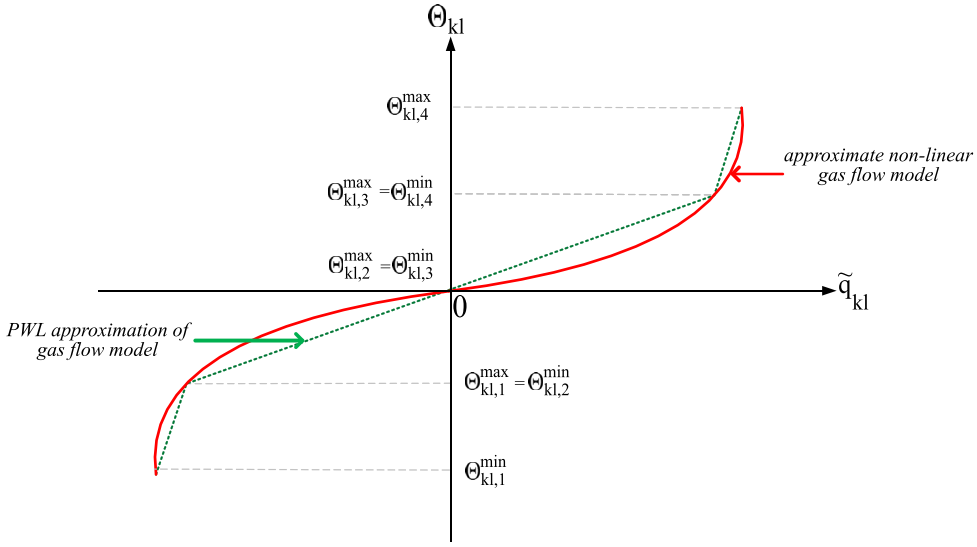

Fig. 3. Piece-wise linearization of approximate non-linear gas flow in (8).

$$\begin{cases} r_{\chi,\kappa}(t) = \dfrac{r_{sk,\chi}(t)}{2} + (-1)^{3-\kappa}\sqrt{r_{ku,\chi}(t) - \dfrac{3}{4}r^2_{sk,\chi}(t)} & \kappa = 1,2 \\ r_{\chi,\kappa}(t) = 0 & \kappa = 3 \end{cases}$$
$$\forall t \in \Omega_T, \forall \chi \in \Omega_\chi \tag{7c}$$

$$\begin{cases} \omega_{\chi,\kappa}(t) = \dfrac{(-1)^{3-\kappa}}{r_{\chi,\kappa}(t)(r_{\chi,1}(t) - r_{\chi,2}(t))} & \kappa = 1,2 \\ \omega_{\chi,\kappa}(t) = \dfrac{1}{m} - \dfrac{1}{r_{sk,\chi}(t) - r^2_{ku,\chi}(t)} & \kappa = 3 \end{cases}$$
$$\forall t \in \Omega_T, \forall \chi \in \Omega_\chi \tag{7d}$$

$$\begin{cases} Z_{\chi,\kappa} = f(\mu_1(t), \mu_2(t), \ldots, e_\kappa(t), \ldots, \mu_{\Omega_\chi}(t)) & \kappa = 1,2 \\ Z_{\chi,\kappa} = f(\mu_1(t), \mu_2(t), \ldots, \mu_\kappa(t), \ldots, \mu_{\Omega_\chi}(t)) & \kappa = 3 \end{cases}$$
$$\forall t \in \Omega_T, \forall \chi \in \Omega_\chi \tag{7e}$$

$$E(Z^c) = \sum_\chi \sum_{\kappa=1}^{2} \left[\omega_{\chi,\kappa}(Z_{\chi,\kappa})^c\right] + \sum_\chi \omega_{\chi,3}(Z_{\chi,3})^c \tag{7f}$$

Step 2.2: Approximate non-linear programming.

In order to simplify the optimization problem and to achieve feasible solutions, gas flow equations in (3) are converted to the approximately non-linear relationship.

EQUATION SET 8 Reformation of Gas Flow Model

$$(\tilde{q}_{kl}(t))^2 = C^2_{kl}.sign(\Theta_k(t), \Theta_l(t)).(\Theta_k(t) - \Theta_l(t)) \qquad \forall t \in \Omega_T \tag{8a}$$

$$sign(\Theta_k(t), \Theta_l(t)) = \begin{cases} 1, & \Theta_k(t) \geq \Theta_l(t) \\ -1, & \Theta_k(t) < \Theta_l(t) \end{cases} \qquad \forall t \in \Omega_T \tag{8b}$$

$$\Theta^{min}_k \leq \Theta_k(t) \leq \Theta^{max}_k \qquad \forall t \in \Omega_T \tag{8c}$$

Although (8a) is a non-linear equation, it is a suitable approximation for the main constraint and improves the feasibility of the objective function.

Step 2.3: Risk analysis.

In our stochastic programming, where uncertainty variables are modeled under the stochastic framework, the total optimal operation cost is uncertain variable specified by a probability value p_ε. Hence, the IPGS is an optimal operation problem involving an uncertain objective function TOC_ε. It is essential to regard a function specifying the distribution of this uncertain variable. This function includes the risk analysis criterion, which is generally utilized in stochastic programming problems [27].

The risk associated with TOC_ε is explicitly captured by incorporating the CVaR metric in the model. In the proposed IPGS optimal operation problem, the coherent value-at-risk (CVaR) is utilized to manage financial risks and uncertainties due to the TOC_ε minimizing. Thus, the objective function in (1) is rewritten as (9).

EQUATION SET 9 Stochastic Co-optimization Model

$$\underset{\substack{P_p, SUC_p, SDC_p \\ G_w, L_{sh}, \xi_\alpha, \ell_\varepsilon}}{Min} \sum_\varepsilon p_\varepsilon . \sum_t \left\{ \sum_p \left[C_p(t).P_p(t,\varepsilon) + SUC_p(t,\varepsilon) + SDC_p(t,\varepsilon)\right] + \sum_w \left[C_g(t).G_w(t,\varepsilon)\right] + VOLL.\sum_i L^i_{sh}(t,\varepsilon) \right\} + \beta.\xi_{CVaR} \qquad \forall t \in T, \forall \varepsilon \in \Omega_E, \forall p \in \Omega_p, \forall w \in \Omega_W \tag{9a}$$

$$\xi_{CVaR} = \xi_\alpha + \frac{1}{1-\alpha}\sum_\varepsilon [\ell_\varepsilon . p_\varepsilon] \qquad \forall \varepsilon \in \Omega_E \tag{9b}$$

subject to (2) − (8)

$$\sum_t \sum_p \left[C_p(t) \cdot P_p(t,\varepsilon) + SUC_p(t,\varepsilon) + SDC_p(t,\varepsilon)\right] + \sum_w \left[C_g(t).G_w(t,\varepsilon)\right] + VOLL \cdot \sum_i L^i_{sh}(t,\varepsilon) - \xi_\alpha \leq \ell_\varepsilon \tag{9c}$$
$$\forall t \in T, \forall \varepsilon \in \Omega_E, \forall p \in \Omega_p, \forall w \in \Omega_W$$

In (9), $\beta \in \mathbb{R}_+$ is the risk-weighted parameter and determines the mutual exchange between cost and risk in different scenarios. The lower amounts of β reduce costs and increase risk, while its large amounts increase costs and reduce risk. Also, the auxiliary variable $\ell_\varepsilon \in \mathbb{R}_+$ determines the range of differences between the TOC and ξ_α in each scenario.

Therefore, the mentioned MINLP is repeated 3^{Ω_x} times in this step. The output of this problem, which is used as input for the Step 3, includes the initial values of Lagrange multiplier in each scenario $\lambda_{ini,\varepsilon}$ and the worst scenario definition among the stochastic scenarios.

EQUATION SET 10 Towards a Mixed Integer Linear Programming Formulation

$$\Theta_{kl,N_{kl}}^{\max} = \Theta_k^{\max} - \Theta_l^{\min} \tag{10a}$$

$$\Theta_{kl,1}^{\min} = \Theta_k^{\min} - \Theta_l^{\max} \tag{10b}$$

$$\tilde{q}_{kl} = \tilde{q}_{kl0} + \sum_{\Im=1}^{N_{kl}} k_{\Im}^{\min} \varpi_{kl,\Im} \tag{10c}$$

$$\Theta_{kl} = \Theta_{kl0} + \sum_{\Im=1}^{N_{kl}} \varpi_{kl,\Im} \tag{10d}$$

$$I_{kl,\Im+1} \cdot \left(\Theta_{kl,\Im}^{\max} - \Theta_{kl,\Im}^{\min}\right) \le \varpi_{kl,\Im} \tag{10e}$$

$$\varpi_{kl,\Im} \le I_{kl,\Im} \cdot \left(\Theta_{kl,\Im}^{\max} - \Theta_{kl,\Im}^{\min}\right) \tag{10f}$$

$$k_{\Im}^{\min} = \frac{\Theta_{kl,\Im} - \Theta_{kl,\Im-1}}{\tilde{q}_{kl,\Im} - \tilde{q}_{kl,\Im-1}} \tag{10g}$$

Step 3: Relaxation.

In Step 2, the MINLP optimization problem is run for different scenarios, and a scenario with the maximum amount of TOC is selected as the worst scenario. In Step 3, the linearization method and SLR approach are applied to the proposed problem. Consequently, the optimization problem of IPGS is solved using relaxed mixed integer programming (RMILP).

Step 3.1: Linearization.

In linear programming, the formulation of the problem is often the least difficult to define. Additionally, numerical methods for solving nonlinear programs have limited information to recognize the global optimum. In this regard, the gas flow constraint of (8a) is non-linear and non-convex, so it is not a completely suitable for the approach. To achieve an MILP model, the piece-wise linear (PWL) approximation method is used. In Ref. [28], a two-dimensional approximation for the gas flow constraint is proposed. In this paper, a one-dimensional approximation for the gas flow constraint is utilized as modeled in (10). Considering $\Theta_{kl}(t) = \Theta_k(t) - \Theta_l(t)$, the range of $\Theta_{kl}(t)$ within $[\Theta_{kl,1}^{\min}\Theta_{kl,N_{kl}}^{\max}]$is divided into a sequence of linear segments N_{kl}. As a result, the non-linear constraint in (8a) is transformed into linear form (10) for fixed time. In Fig. 3, a schematic of piece-wise linearization is illustrated for $N_{kl} = 4$. Corresponding nodal pressure squared, the operating interval is specified by maximum and minimum parameters incorporating to predefined sub-intervals. The number of segments can be adjusted in order to reduce the breakpoints or improve the solution quality. In fact, increasing the number of segments results in accurate solution while the problem has low computational speed and high calculation complexity as well as needs to define additional variables.

Step 3.2: Lagrange relaxation.

LR is a powerful relaxation approach that is used in optimization problems. In the mentioned optimization problems, due to a large number of constraints and variables, the main problem is converted to its dual. So, the complicated constraints are added as penalty terms to the objective function. The penalty term includes dual variables of Lagrange multipliers and produces a lower bound for the problem [29].

EQUATION SET 11 Surrogate Lagrange Relaxation Method

$$\underset{x}{Min} \sum_n \left[c_{1,n}x_n + c_{2,n}y_n\right] \qquad \forall n \in \Omega_N, y_n \in \{0,1\} \tag{11a}$$

$$s.t. \sum_n \left[A_{1,n}x_n + A_{2,n}y_n\right] = b \qquad \forall n \in \Omega_N, y_n \in \{0,1\} \tag{11b}$$

$$\sum_n \left[A_{3,n}x_n + A_{4,n}y_n\right] \le d \qquad \forall n \in \Omega_N, y_n \in \{0,1\} \tag{11c}$$

$$LD(\lambda) = b\lambda + \sum_n Z_n(\lambda) \qquad \forall n \in \Omega_N, y_n \in \{0,1\} \tag{11d}$$

$$\underset{x}{Min}\, Z_n(\lambda) = c_{1,n}x_n + c_{2,n}y_n - \lambda^{\tau}\left[A_{1,n}x_n + A_{2,n}y_n\right]$$
$$\forall n \in \Omega_N, y_n \in \{0,1\} \tag{11e}$$

$$\underset{x}{Max}\, LD(\lambda) \tag{11f}$$

The new formation of the mentioned problem after applying the linearization process comes as (11a)-(11c) for a fixed time. x_n, y_n are regarded as decision variables for subscript n. By applying the duality approach and SLR, Lagrangian dual $LD(\lambda)$ of the problem is defined as (11d). Dual variables λ are utilized as multipliers for relaxing complicated constraints. In addition, $Z_n(\lambda)$ is calculated by (11e). Due to the nature of the minimization of the problem, it is necessary to find the lower bound that comes from (11f).

The master problem (MP) consists of the linear objective function (1), the equality constraints (2a), (2b), (2e), (2f), (2m), (2r), (2s), (3d), (4a), (4b), (4e), (4f), (5c), (5e)-(5j), (6a), (6b) and (10a)-(10d), the inequality constraints (2 g)-(2i), (3e), (10e) and (10f) as well as the capacity constraints (2c), (2d), (2j), (2k), (2l), (2n)-(2q), (3f), (3 g), (4c), (4d), (6c), and (6d). The most important challenge is its large scale. Hence, MP is decomposed into several SPs and is solved by the B&C method [30]. To coordinate between SPs, the SLR approach is applied [31]. The advantages of the SLR are no need for performing the complete optimization of the relaxed problem and no need for the optimal value of the dual problem. Therefore, according to the proposed formulas for the IPGS optimization problem, by relaxing two complicated constraints including power flow (2b) and gas flow (10f), the objective function of the problem is rewritten as (12a). To indicate the linearity of the problem, $\tilde{q}_{kl}^2(t)$ is replaced by $\tilde{q}_{kl}(t)$. In this dual problem, $\lambda_1(t)$ and $\lambda_2(t)$ are Lagrange multipliers for the constraints of power and gas flow, respectively. The relaxed relation in (12a) is decomposed into SP1 and SP2 subproblems. The optimal value obtained from the (12b) is shown by $L(\lambda_1(t), \lambda_2(t))$ and is replaced in the (12c).

EQUATION SET 12 Duality Approach

$$
\begin{aligned}
&Min \sum_t \left\{ \sum_p \left[C_p(t).P_p(t) + SUC_p(t) + SDC_p(t) \right] \right\} \\
&+ \sum_w \left[C_g(t).G_w(t) \right] + VOLL.\sum_i L^i_{sh}(t) \Bigg\} \\
&+ \lambda_1(t).\left[\sum_i \sum_j P_{ij}(t) - \sum_i \sum_j \frac{\delta_i(t) - \delta_j(t)}{x_{ij}} \right] + \\
&\lambda_2(t).\left[\sum_k \sum_l \tilde{q}_{kl}(t) - \right. \\
&\left. \sum_k \sum_l C_{kl}.sign(\Theta_k(t), \Theta_l(t)).(\Theta_k(t) - \Theta_l(t)) \right] \\
&\forall t \in T, \forall p \in \Omega_p, \forall w \in \Omega_W
\end{aligned}
\tag{12a}
$$

$$
\begin{aligned}
&SP1: = \underset{\substack{P_p, SUC_p \\ SDC_p, L_{sh}}}{Min} \sum_t \left\{ \sum_p \left[C_p(t).P_p(t) + SUC_p(t) + SDC_p(t) \right] + \right. \\
&\sum_w \left[C_g(t).G_w(t) \right] + VOLL.\sum_i L^i_{sh}(t) - \\
&\lambda_1(t).\sum_i \sum_j \frac{\delta_i(t) - \delta_j(t)}{x_{ij}} - \\
&\left. \lambda_2(t).\sum_k \sum_l C_{kl}.sign(\Theta_k(t), \Theta_l(t)).(\Theta_k(t) - \Theta_l(t)) \right\} \\
&\forall t \in T, \forall p \in \Omega_p, \forall w \in \Omega_W
\end{aligned}
\tag{12b}
$$

$$
\begin{aligned}
SP2 := \underset{\lambda_1, \lambda_2}{Max} \quad & \sum_t \left\{ L(\lambda_1(t), \lambda_2(t)) + \lambda_1(t).\sum_i \sum_j P_{ij}(t) + \right. \\
& \left. \lambda_2(t).\sum_k \sum_l \tilde{q}_{kl}(t) \right\} \qquad \forall t \in T
\end{aligned}
\tag{12c}
$$

Proposed methodology is summarized in Fig. 4.

5. Numerical results

In order to verify the efficiency of the proposed method, a cost-effective optimization approach for IPGS operation is presented in which the price values have considerable effects on the performance of components. The relation between price fluctuation and components' operation is explained as follows. The price increase results in a decrease of the received power from TGs; however, at the low-cost hours, the generated power from them is increased. Thus, the operation of TGs has an inverse relation with the price. On the other hand, the generated power from GTs is significantly increased for supporting TGs at high-cost hours. In contrast, the GTs function at their low capacity by energy price decreasing. Hence, the operation of GTs has a direct relation with the price. Additionally, ES is charged for low-price periods and discharged for high-price intervals. Also, low-cost energy is consumed by P2G to generate gas and increase power system profit. Furthermore, the generated energy by electric power supplies (in particular RESs) is consumed for load demand at the high-cost hours.

The proposed method is validated in two case studies: a 6-bus power system connected with a 7-node NG network (Case study 1) and IEEE RTS 24-bus system connected with the Belgian NG network (Case study 2). For Step 1 and Step 2, the proposed MINLP optimal operation problem is solved with CONOPT solver. To apply the B&C method, the CPLEX solver is utilized for solving the MILP problem in Step 3. The entire process is done via GAMS software in a personal computer with Intel processor CPU 2.67 GHz.

5.1. Case study 1

The 6-bus power system integrated with 7-node NG system shown in Fig. 5 is studied. The 6-bus power system includes three TGs, one WT, one PV, one ES, seven transmission lines, and three loads. The WT connected to the bus 2 has $P^{max}_{WT} = 100$ MW. The capacity of ES is 200 MWh. Also, $P^{max}_{ch} = P^{max}_{dch} = 20$ MW, $P^{min}_{ch} = P^{min}_{dch} = 0$ and $\eta_{ch} = \eta_{dch} = 90\%$. It is worth to note that in this process *SOC(1)* must be equal to *SOC(24)*. In addition, the PV connected to the bus 1 has $P^{max}_{PV} = 50$ MW. The 7-node NG network includes two gas wells, one compressor, and six pipelines. To integrate the power system and NG network two GTs and one P2G are utilized as the joint units. Also, the P2G with a maximum capacity of 100 MW connects bus 2 to node 1. The profiles of wind speed, solar radiation, load and price are illustrated in Fig. 6 [32]. Other data can be found in Ref. [26]. The following results are illustrated for a random-selected scenario.

The operation principles of joint units were analyzed for showing the benefits of IPGS. In this regard, Fig. 8 illustrates the effects of utilizing GTs. Accordingly, the TGs in the conventional independent power systems are always on within a day. In contrast, by making coordination between the power system and NG network and utilizing GTs, the pressure on TGs is significantly decreased. As a result, GTs almost supply the load, and TGs operate almost in peak times [17,22]. According to Fig. 8, the power generators TG3 and GT2 are always on because of high demand power in the bus 1 and proper gas pressure in node 2 by utilizing compressor through the pipeline PL2. Utilizing P2G not only enhances the power systems profit by selling gas to the NG network but also, by consuming curtailment power of WT provides energy saving. Fig. 9 shows the curtailment power of WT wasted in the independent power system. However, this power is completely consumed in the IPGS for generating NG by utilizing P2G. As another result, the optimal operation of ES is shown in Fig. 7. It is clear that the SOC of ES is increased within low energy price hours and decreased at low energy price hours.

5.2. Case study 2

For numerical analysis, IPGS is modeled as IEEE RTS 24-bus system connected with the Belgian NG network as presented in Fig. 10. Through the four GTs (Ω_{GT}=4) with maximum capacity 152 MW, 152 MW, 155 MW and 300 MW, nodes Sinsin, Petange, Voeren, and Loenhout are connected to buses 1, 2, 16 and 20, respectively. The efficiency of the GTs is $\eta_{GT} = 90\%$, the stand-alone IEEE RTS 24-bus system supplies the load with $\Omega_{TG} = 8$. The detailed technical data of TGs and GTs as well as electrical load are presented in Table 1, Table 2 and Table 3, respectively. It is note to worth that in this practical case study all power generators operate at least by their minimum power. Also, the time step of RU, RD, SU, and SD is an hour. Other related data is available in Ref. [33]. Four wind turbines (ω_{WT}=4) with nominal powers $P^{max}_{WT,1} = 200$ MW, $P^{max}_{WT,2} = 150$ MW, $P^{max}_{WT,3} = 100$ MW and $P^{max}_{WT,4} = 200$ MW are connected to buses 8, 19, 21 and 3, respectively. According to Ref. [34], the average wind speed at 50-m height is considered to be 5.12 m/s. Values of v_{ci} and v_{co} are considered to be 2 m/s and 8 m/s, respectively. Also, two P2G units (Ω_B=2) as power plants [35] are installed nearby WTs between buses 17,24 and nodes Zomegem and Liege, respectively. The reason for considering P2G near WT is reaching to most utilization of the curtailment power of wind turbine [36,37]. The maximum capacity of P2Gs is 30 MW and

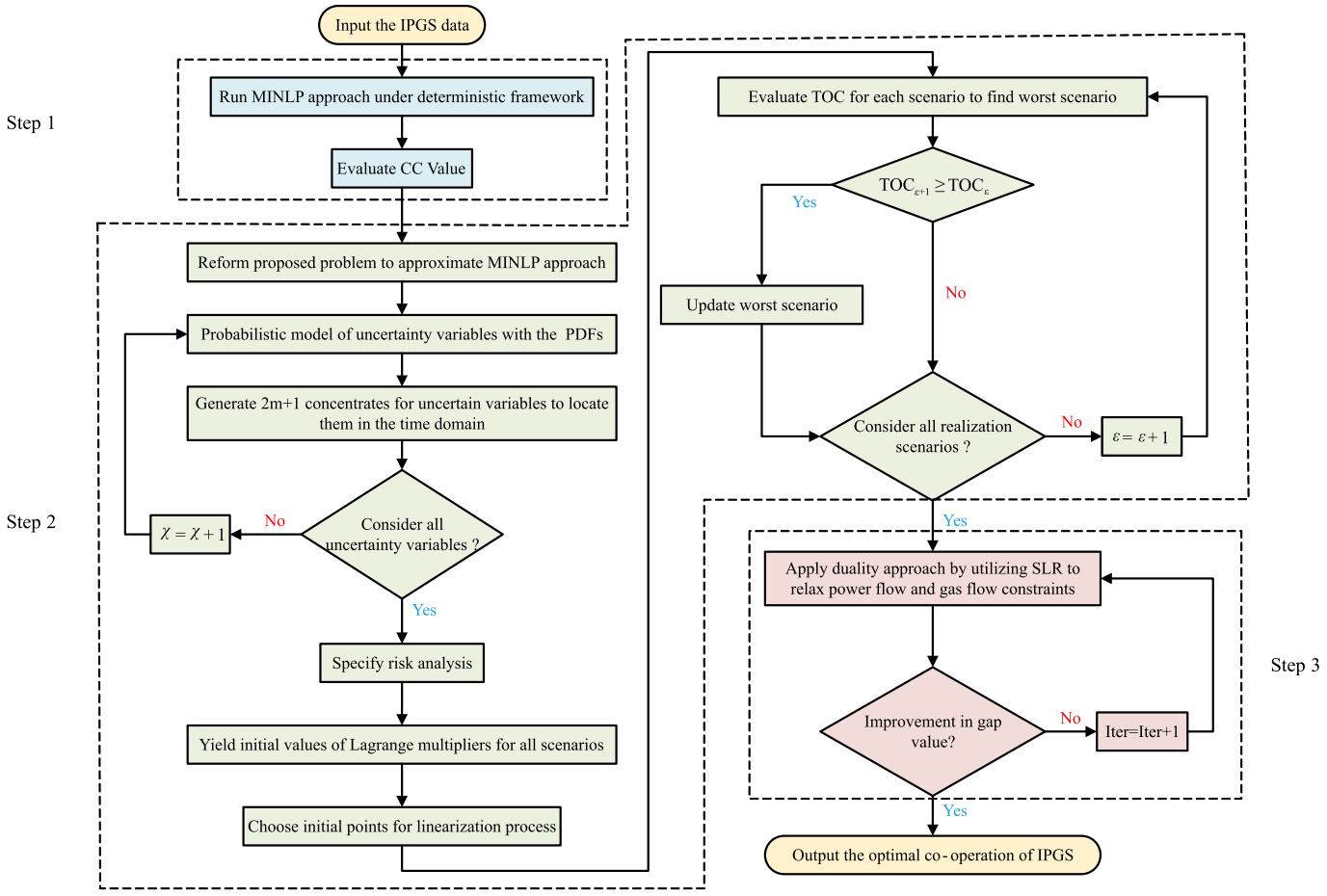

Fig. 4. Problem-solving process using the proposed series multi-step model.

70 MW with $\eta_{P2G} = 70\%$. According to Ref. [38], the average radiation level in Belgium is 4.61 kWh/m^2. As shown in Fig. 10, the number of PVs is $\Omega_{PV} = 2$ which the maximum capacity of them is $P^{max}_{PV,1} = 50$ MW and $P^{max}_{PV,2} = 100$ MW. In addition, the number of ESs is $\Omega_{\rho} = 2$ with the capacity of 200 MWh and 100 MWh. Also, $P^{max}_{ch,1} = P^{max}_{dch,1} = 20$ MW and $P^{max}_{ch,2} = P^{max}_{dch,2} = 10$ MW. Other characteristics of ESs are same as the case study 1. Furthermore, the input data in Fig. 6 is utilized as basic deterministic scenarios in which profile of wind speed and solar radiation are related to 8 m/s and 4.61 kWh/m^2, respectively.

To integrate a power system with an NG network and to avoid dysfunction in supplying electrical loads and NG loads by their own infrastructures, there is a need to determine the CC value. In this order, the MINLP problem is solved under the deterministic framework. The operation of joint units has an important role in the power system and NG network interconnecting. Indeed, the consumed power by P2Gs and consumed gas by GTs are the main factors for determining CC value. Interconnected nodes might vary depending on the topology of the IPGS and operational constraints. So, the system's planner/operator can change these joint nodes. According to Fig. 10, it is assumed that there are 6 joint nodes-buses. Further, the energy exchange values are provided only for the interconnected nodes, as only these nodes have coordination capacity of the joint units (GTs and P2Gs). Fig. 11 shows the transferred power from power system to NG network. In addition, received power from NG network to power system is presented as Fig. 11. In our approach, all objective functions and constraints are linear except for gas flow relation in (3), which is linearized in (8)

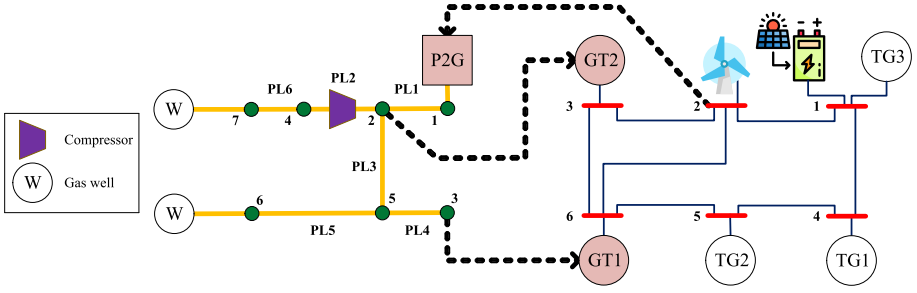

Fig. 5. Interconnection between 6-bus power system and 7-node NG network.

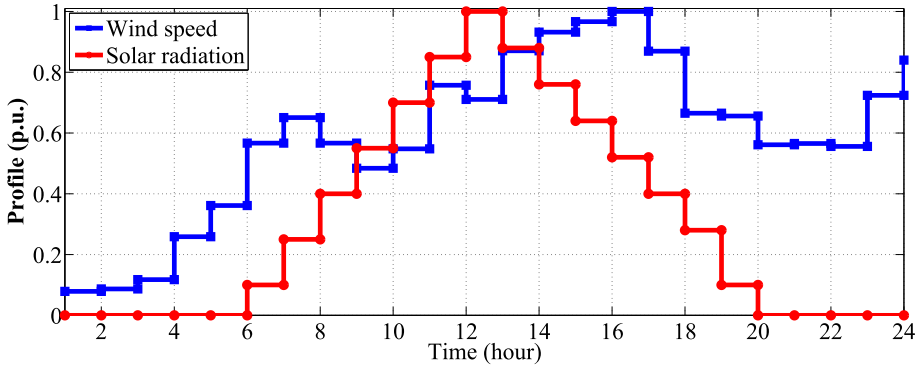

(a)

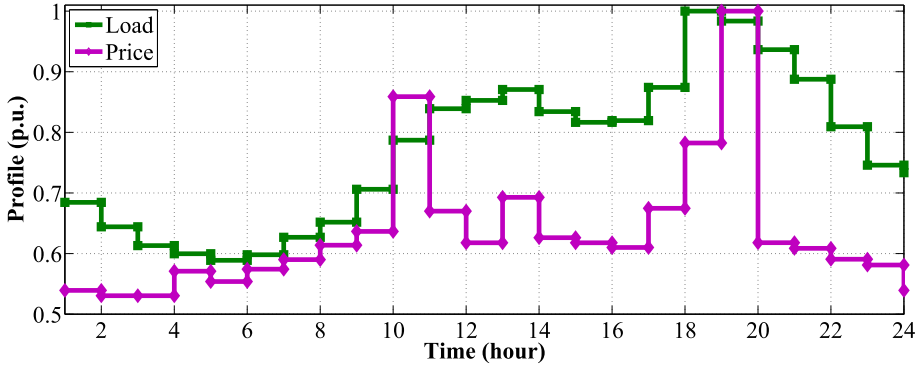

(b)

Fig. 6. Normalized input data by their predefined maximum values. (a) Wind speed and solar radiation profiles. (b) Load and price profiles.

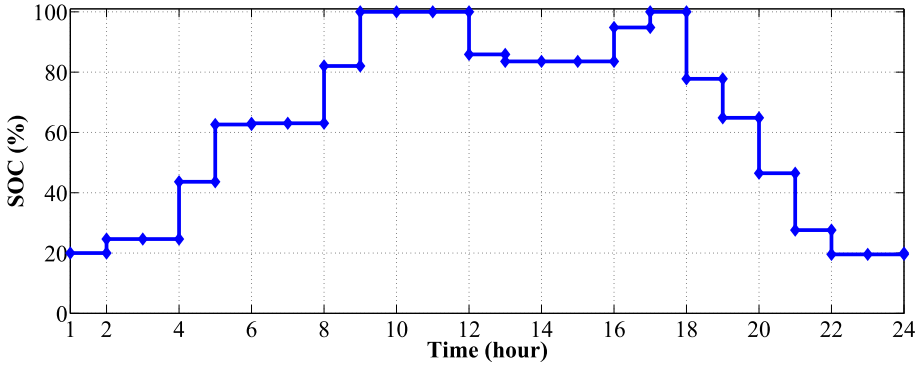

Fig. 7. State of charge of ES in case study 1.

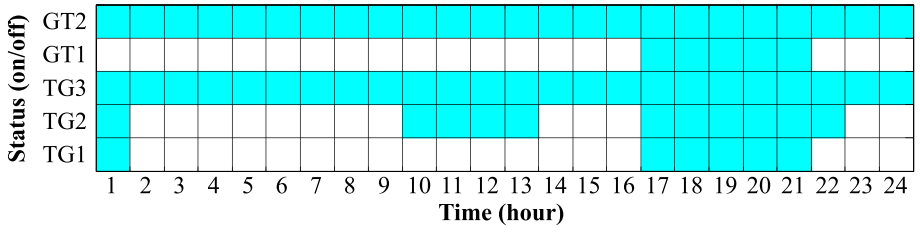

Fig. 8. Operation status of generators.

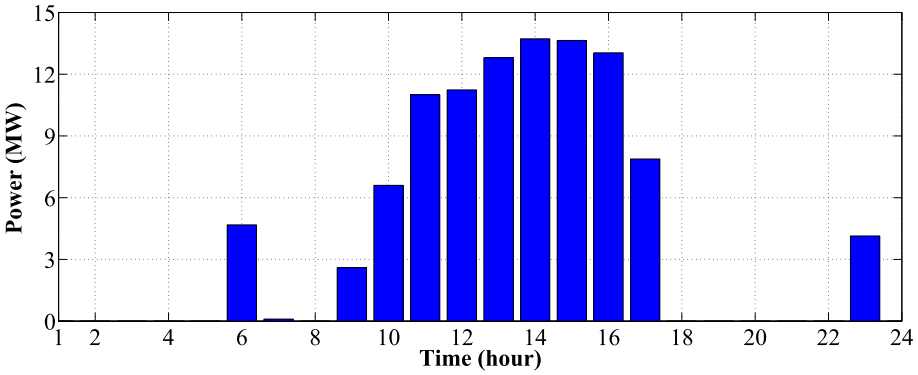

Fig. 9. Curtailment power of the WT for independent power system.

and (10). Considering the linear programming methodology and the aforementioned statements about coordination capacity, we conclude that the variations of $\partial_{GT}(t)$ and $\partial_{P2G}(t)$ are linear. To determine the values of $\partial_{GT}(t)$ and $\partial_{P2G}(t)$, we solve the IPGS optimization problem regarding the gas flow in the pipelines and power flow in the lines. So, there is a tight relationship between the way of energy flow and coordination capacity. Accordingly, within one day the transferred and received energy by power system are 1425 MWh and 9944 MWh, respectively.

With the incorporation of CC value, the optimal operation of IPGS under a stochastic framework is solved. On the one hand, three WTs and two PVs are installed in the proposed power system, and on the other hand, the fluctuate of the electrical load is uncertain. As a result, the number of uncertainty variables is $\Omega_\chi = 6$. Thus, to produce realization scenarios, there is a need for a six-stage process, as illustrated in Fig. 2. Indeed, by generating 1000 scenarios for wind speed, solar radiation, and load profile and applying $2m + 1$ PEM approach, finally, 3^6 scenarios are produced to realize the stochastic nature of IPGS operation. As a sample result, the generation power from GTs and consumed power by P2G for a random-selected scenario are illustrated in Fig. 12. Indeed, each P2G operates as a load for the power system, and each GT operates as a power supply. Regarding the data in Fig. 6, the operation of joint units are highly affected by the load profile and RESs generated power. Also, the SOC variation of ESs illustrated in Fig. 13. Accordingly, there is a tightly relation between ESs operation and price.

Different parts of the understudy IPGS are analyzed from the operation cost point of view in Table 4. The proposed stochastic operation co-optimization problem is solved for various standard deviations of the uncertainty variables. From this table, it is clear that the TOC of the IPGS is increased by the standard deviation. However, The TOC growth with increasing uncertainty level is verified by the value of the stochastic solution, as explained in Ref. [27]. For instance, the deterministic value of TOC, its optimal values for $\sigma = 3\%$, 8% and 10% has 6.2%, 6.7% and 7% growth, respectively. In addition, for each σ the marginal difference between TOC of the worst-scenario and TOC of the best-scenario is changed. In fact, increment in the standard deviation causes infeasible solutions and increases financial risk. As presented in

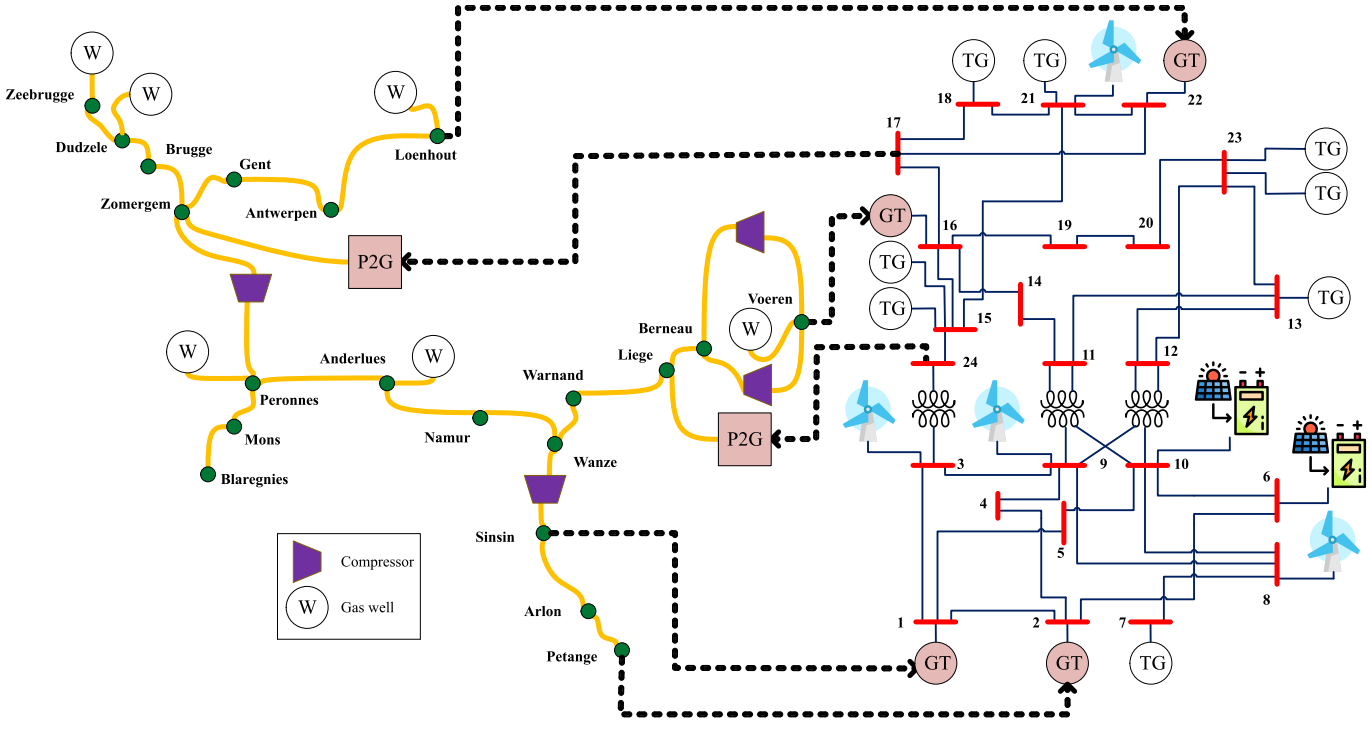

Fig. 10. Interconnection between IEEE RTS 24-bus and Belgian NG network.

Table 1
Technical data of GTs.

bus	$P^{max}_{GT,gt}$ (MW)	$P^{min}_{GT,gt}$ (MW)	RU_{gt} (MW)	RD_{gt} (MW)	SU_{gt} (MW)	SD_{gt} (MW)
1	152	11	24	24	43	45
2	152	32	24	24	44	57
16	155	24	31	31	66	73
22	300	0	35	35	315	326

Table 2
Technical data of TGs.

bus	$P^{max}_{TG,gt}$ (MW)	$P^{min}_{TG,tg}$ (MW)	RU_{tg} (MW)	RD_{tg} (MW)	SU_{tg} (MW)	SD_{tg} (MW)
7	350	75	94	49	77	80
13	550	20	24	24	213	228
15	155	44	31	31	66	73
15	300	0	35	35	315	326
15	155	55	21	21	112	125
18	400	100	45	45	115	126
21	400	100	45	45	115	126
23	300	110	21	21	112	125
23	350	75	49	49	77	80

Table 3
The maximum load demand of the IEEE RTS 24-bus in each bus.

bus	1	2	3	4	5	6	7	8	9	10	13	14	15	16	18	19	20
$P^{i,max}_{d}$ (MW)	108	97	180	74	71	136	125	171	175	195	265	194	317	100	333	181	128

Table 4, for each σ the TOC of the worst-scenario is more than TOC of other scenarios. Correspondingly, the value of TOC in the worst-scenario for σ = 10% is increased by almost 8% and 9% for the optimal and best scenario, respectively. Similarly, the generated power from GTs in the worst scenario is more than other scenarios. So, with increasing uncertainty level, the power system requires more NG. Since the power system priority is to supply its own load (P_d), the consumed power from P2G units in the worst-scenario is less than two other scenarios for each σ. As expected, the consumed power by the P2G units in the best-scenarios (which have more generated power from RESs and less load demand) is more than other scenarios for each σ. As another important result from this table, the uncertainty variables have no influence on TGs operation. In fact, the imbalances between generated power from RESs and load are compensated by the interconnection between the power system and NG network. To achieve equilibrium between supply and demand and to eliminate the shaded load, the consumed gas of GTs is increased, and consumed power by P2G units is decreased. Therefore, the power system flexibility and robustness are improved against uncertainty variables by joint units.

In the proposed scenario-based stochastic operation co-optimizing, the number of scenarios has a significant impact on TOC. The GAMS/Scenred2 command is employed for sampling among the 3^6 realization scenarios [27]. Applying Scenred2 requires a special formulation of the stochastic programming model, as stated in (9). Probabilistic information must be given by a set of nodes implying a certain ancestor structure, including a well-defined root node similar to Fig. 2. According to the results in Table 4, the value of TOC in the deterministic framework is 5.624×10^5 $. However, with incorporating uncertainty variables, the value of TOC has increased. The considered number of scenarios has a direct relation with this increase. As presented in Table 5, The value of TOC for scenario numbers between 5 and 200 increases by 4.4%; however, for the scenario numbers within the range of 200–725, the TOC variation rate is about 0.3%. Accordingly, the optimal value of TOC is saturated by scenario number increment.

For risk analysis under a stochastic framework, the CVaR values are used, as stated in (9). The confidential level (α) is set at 95%. In fact, the decision-maker has confidence in the 95% realization scenarios, and the goal of risk analysis is managing the rest of them. The inverse relation between optimal operation and financial risks for different risk levels is evaluated. The effect of risk analysis on TOC and CVar for different values of the parameter β is illustrated in Fig. 14. The minimum value of TOC is 6.02×10^5 $ for β = 0. The latter

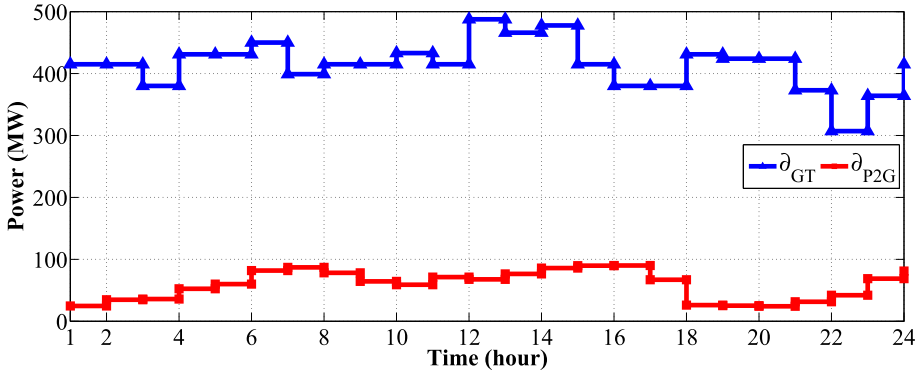

Fig. 11. Exchanged power between power system and NG network to determine CC.

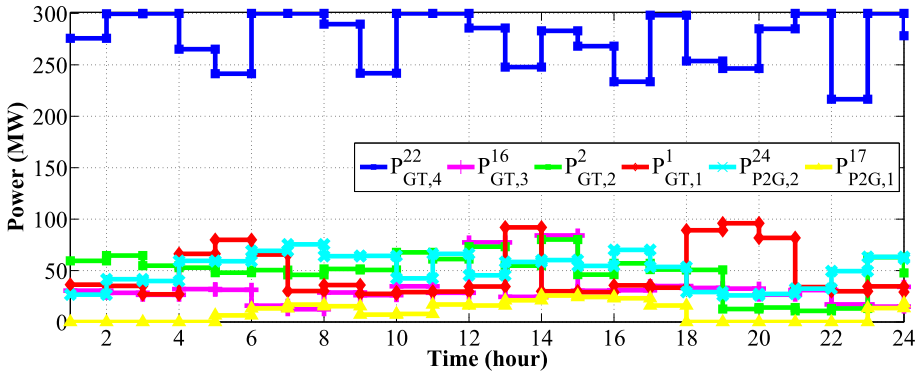

Fig. 12. Generated power by GTs and consumed power by P2Gs in the joint buses for a sample scenario.

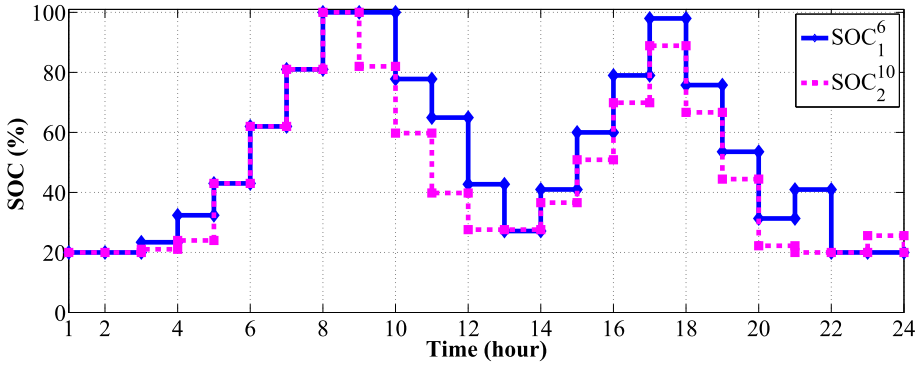

Fig. 13. State of charge of ES in case study 2.

Table 4
Operation cost of various components in IPGS with different standard deviation and $\beta = 0.2$ ($\$ \times 10^5$).

	Deterministic	$\sigma = 3\%$			$\sigma = 8\%$			$\sigma = 10\%$		
		worst scenario	optimal	best scenario	Worst Scenario	optimal	best scenario	worst scenario	optimal	best scenario
p_ε (%)	100	0.141	–	0.136	0.106	–	0.119	0.122	–	0.091
P_{TG}	4.951	5.18	5.18	5.18	5.18	5.18	5.18	5.18	5.18	5.18
P_{GT}	0.628	0.734	0.720	0.716	0.782	0.760	0.724	1.334	0.800	0.690
P_{P2G}	0.045	0.070	0.072	0.080	0.058	0.065	0.068	0.050	0.056	0.066
TOC	5.624	5.98	5.972	5.974	6.030	6	5.972	6.564	6.020	5.936

demonstrates that the decision-maker is a risk-taker who will minimize its TOC without incorporation any financial risks. Inversely, by increasing β the decision-maker becomes more risk-averse, and it leads to the higher TOCs. Furthermore, to analyze the effect of confidential level variation on the costs of IPGS, the values of TOC and CVaR are compared in Table 6. Varying the α value from 85% to 99% leads to increase of IPGS costs. The extreme case of α equal to 99% translates an over cut-off point, requiring the constraint satisfaction for every possible demand profile. Summing up, choosing greater α leads to safer but more expensive operation.

In order to make the proposed problem tractable by efficient MILP solvers, the non-linear gas flow constraint needs to be linearized. In this regard, an one-dimensional PWL approximation is used for worst-scenario with $\sigma = 10\%$ as illustrated in Fig. 3. Then, to efficiently solve large-scale MILP problem in a relatively short time, the SLR approach is specialized for the proposed large scale co-optimization problem. Fig. 15 shows a comparison between different solution methods for MILP operation co-optimization of the IPGS. It is clear that the convergence speed and computation efficiency of SLR are significantly more suitable than pure B&C solution. The best known feasible cost is achieved at 1.04 s by pure B&C approach while the lower bounds with proper gaps are obtained relatively faster than by applying different SLR methods. The SLR methods in terms of Lagrange multipliers initialization and relaxation degree are compared, as well. Indeed, in "SLR1″ just gas flow constraint is relaxed, and power flow constraint is excluded from the dual objective function. However, in "SLR2″ both gas flow and power flow constraints are relaxed. To show the effectiveness of the proposed series multi-step method, the determination of initial values for $\lambda_1(t)$ and $\lambda_2(t)$ are compared by denoting "I″ for initialization and "NI" for non-initialization. Accordingly, the gap of SLR2+B&C + NI is 1.1% more than SLR2+B&C + I. In addition, the convergence speed of SLR2+B&C + I is faster than both SLR2+B&C + NI and SLR2+B&C + I.

The detailed numerical comparison is highlighted in Table 7. The significant enhancement in response speed is achieved by employing SLR method. Also, the effect of utilizing initialized values from the previous step causes improvement in both convergence

Table 5
Effect of scenario number increment on operation cost of IPGS with $\sigma = 10\%$.

Scenario number	5	10	50	100	200	500	729
TOC ($\$ \times 10^5$)	5.748	5.910	5.974	5.988	6.001	6.019	6.020

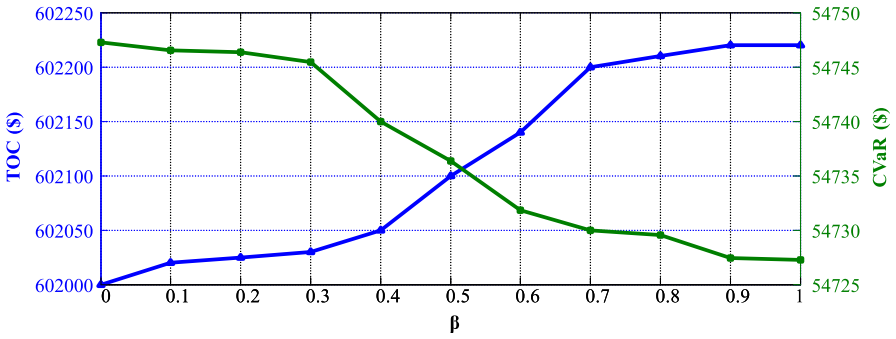

Fig. 14. Comparison of TOCs and CVaRs at different risk levels with $\alpha = 95\%$ and $\sigma = 10\%$.

time and gap, which is verification for the proposed series multi-step approach. In addition, SLR2+B&C + I reaches to a feasible solution faster than SLR1+B&C + I. However, the gap of SLR2+B&C + I is smoothly more than SLR1+B&C + I. Thus, it depends on the operator to make the best choice between these alternatives.

In Fig. 16, the load shed value is analyzed under different rates of CC and γ. Correspondingly, 49.98 MW of load is lost for separate operating as well as without RESs. Furthermore, with 100% penetrating of RESs these load losses are decreased to 11.66 MW. In contrast, the significant improvement in L_{sh} is achieved by integrating between power system and NG network. In fact, the value of L_{sh} is 0.2 MW when RESs are completely eliminated. Consequently, to compensate L_{sh} and to improve the reliability of the power system, the integration is more efficient and applicable than RESs installation. This finding is validation for the importance of integrating the power and NG system. It should be noted that a significant reduction in the TOC (because of VOLL removing) compensates the costs of purchasing, installing, and maintaining joint units.

Table 6
Comparison of TOCs and CVaRs at different confidential level with $\beta = 50\%$ and $\sigma = 10\%$.

α (%)	TOC ($)	CVaR ($)
75	590601	52580
80	593019	52822
85	601840	53705
90	607341	54256
95	612100	54735
99	619221	55447

6. Conclusion

This paper presents the potential of SLR application as a fast solution for IPGS optimal co-operation problem, which is mainly benefited from the series multi-step approach. Through the proposed method, the non-linear and complicated constraints are relaxed such that the proposed problem is converted to separate SPs, which can be solved efficiently. In this iterative method, for the worst scenario, the SPs feeds back to the MP until the gap of TOC

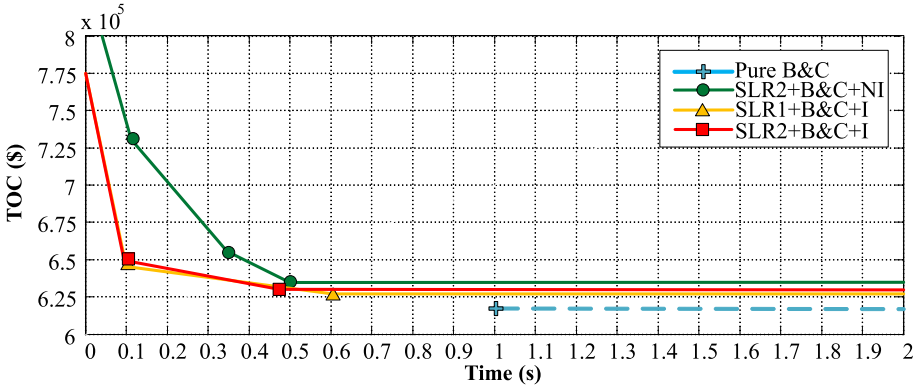

Fig. 15. Comparison of pure B&C solution and various SLR solutions for IPGS optimal co-operation problem.

Table 7
Comparison of different approaches to solve proposed problem.

Problem	base MINLP	MILP			
Approach	–	pure B&C	SLR1+B&C + I	SLR2+B&C + I	SLR2+B&C + NI
Solver	CONOPT	CPLEX			
CPU time (s)	20.51	1.04	0.49	0.47	0.61
TOC ($)	656427	623580	626074	627321	632933
GAP (%)	–	0	0.4	0.6	1.5

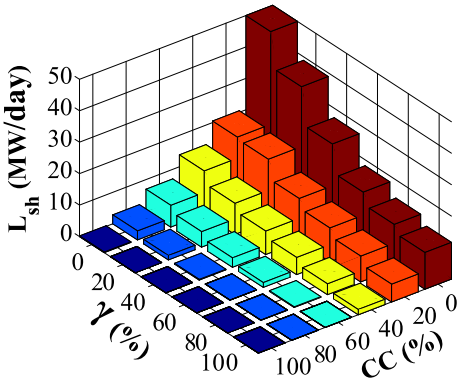

Fig. 16. Illustration of shaded load variation against RESs penetration and coordination capacity rates.

cannot be improved. Furthermore, to avoid the poor computational performance of MINLP, a two-dimension PWL gas flow model was utilized to resolve the problem as a MILP problem. A scenario-based stochastic decision-making model incorporating the CVaR scheme is adjusted for analyzing the financial risk.

According to the numerical results, the proposed method for solving IPGS optimal co-operation problem offers a feasible solution and proper objective value. Moreover, the method has a remarkably higher computing speed compared with the non-relaxed MILP and other SLR methods. Also, it is concluded that the energy exchange between the power system and NG network provides the desired solution to solve the impact of uncertainties in the IPGS. The generated curtailment power from WTs can be utilized by the P2G units for injecting synthetic gas to the NG network at the time interval of the valley or normal load demand. According to the results from risk analyses, there is a trade-off between cost increase and reliability that the decision-maker might be willing to evaluate. The proposed approach provides a tool to choose the best combination. Additionally, our paper quantifies the impact of RESs penetration and CC value on the L_{sh} in which IPGS can supply the demand with lower TOC by increasing in the CC value.

The proposed series multi-step approach can be easily expanded to other problems like planning [8], economic dispatch [39], and energy market [21]. Further researches will include the transient gas flow model, deep focusing on ESs operation, and expanding this method for long term operation.

CRediT authorship contribution statement

Behdad Faridpak: Conceptualization, Methodology, Software, Validation, Formal analysis, Data curation, Writing - original draft, Writing - review & editing, Visualization. **Meisam Farrokhifar:** Supervision, Investigation, Conceptualization, Methodology, Validation, Formal analysis, Data curation, Writing - original draft, Writing - review & editing, Visualization. **Ilgiz Murzakhanov:** Conceptualization, Methodology, Formal analysis, Writing - original draft, Writing - review & editing, Visualization. **Amin Safari:** Conceptualization, Methodology, Formal analysis, Writing - review & editing, Visualization.

References

[1] Guelpa E, Bischi A, Verda V, Chertkov M, Lund H. Towards future infrastructures for sustainable multi-energy systems: a review. Energy 2019;184:2–21.
[2] Correa G, Muñoz P, Rodriguez C. A comparative energy and environmental analysis of a diesel, hybrid, hydrogen and electric urban bus. Energy 2019;187:115906.
[3] Latifi H, Farrokhifar M, Safari A, Pournasir S. Optimal sizing of combined heat and power generation units using of MPSO in the Besat industrial zone. Int J Energy and Stat 2016;4(1):1650002.
[4] Zhou H, Zheng J, Li Z, Wu Q, Zhou X. Multi-stage contingency-constrained co-planning for electricity-gas systems interconnected with gas-fired units and power-to-gas plants using iterative Benders decomposition. Energy 2019;180:689–701.
[5] Bashardoust A, Farrokhifar M, Fard AY, Safari A, Mokhtarpour E. Optimum network reconfiguration to improve power quality and reliability in distribution system. Int J Grid and Distributed Comput 2016;9(4):101–10.
[6] Ćosić B, Krajačić G, Duić N. A 100% renewable energy system in the year 2050: the case of Macedonia. Energy 2012;48(1):80–7.
[7] Farrokhifar M, Mahaei SM, Jafarzadeh J, Gholami M. Distribution networks reconfiguration for loss minimization based on variable behavior of loads and energy cost curves. In: In 39th annual conference of the IEEE industrial electronics society; 2013. p. 2022–6.
[8] Nie Y, Farrokhifar M, Pozo D. Electricity and gas network expansion planning: an ADMM-based decomposition approach. In: IEEE PowerTech; 2019.
[9] Farrokhifar M, Nie Y, Pozo D. Energy systems planning: a survey on models for integrated power and natural gas networks coordination. Appl Energy 2020;262:114567.
[10] Zhou S, Zhuang W, Wu Z, Gu W, Zhan X, Liu Z, Cao S. Optimized scheduling of multi-region Gas and Power Complementary system considering tiered gas tariff. Energy 2020;193:116677.
[11] Chen X, Wang C, Wu Q, Dong X, Yang M, He S, Liang J. Optimal operation of integrated energy system considering dynamic heat-gas characteristics and uncertain wind power. *Energy*; 2020. p. 117270.
[12] He C, Wu L, Liu T, Wei W, Wang C. Co-optimization scheduling of interdependent power and gas systems with electricity and gas uncertainties. Energy 2018;159:1003–15.
[13] Qu K, Zheng B, Yu T, Li H. Convex decoupled-synergetic strategies for robust multi-objective power and gas flow considering power to gas. Energy 2019;168:753–71.
[14] Yang L, Zhao X, Li X, Feng X, Yan W. An MILP-based optimal power and gas flow in electricity-gas coupled networks. Energy Procedia 2019;158:6399–404.
[15] Dokic SB, Rajakovic NL. Security modelling of integrated gas and electrical power systems by analyzing critical situations and potentials for performance optimization. Energy 2019;184:141–50.
[16] Khani H, Farag HEZ. Optimal day-ahead scheduling of power-to-gas energy storage and gas load management in wholesale electricity and gas markets. IEEE Trans Sustain Energy 2018;9(2):940–51.
[17] Zhang Y, Huang Z, Zheng F, Zhou R, Le J, An X. Cooperative optimization scheduling of the electricity-gas coupled system considering wind power uncertainty via a decomposition-coordination framework. Energy 2020;194:116827.
[18] Zahedi Rad V, Torabi SA, Shakouri G H. Joint electricity generation and transmission expansion planning under integrated gas and power system. Energy 2019;167:523–37.
[19] Faridpak B, Alahyari A, Farrokhifar M, Momeni H. Toward small scale renewable energy hub-based hybrid fuel stations: appraising structure and scheduling. IEEE Trans Transport Electrification 2020;6(1):267–77.
[20] Gao J, Ma Z, Guo F. The influence of demand response on wind-integrated power system considering participation of the demand side. Energy 2019;178:723–38.
[21] Qiu J, Zhao J, Yang H, Dong ZY. Optimal scheduling for prosumers in coupled transactive power and gas systems. IEEE Trans Power Syst 2018;33(2):1970–80.
[22] Yamchi HB, Shahsavari H, Kalantari NT, Safari A, Farrokhifar M. A cost-efficient application of different battery energy storage technologies in microgrids considering load uncertainty. J Energy Storage 2019;22:17–26.
[23] Piacentino A, Duic N, Markovska N, Mathiesen BV, Guzović Z, Eveloy V, Lund H. Sustainable and cost-efficient energy supply and utilization through innovative concepts and technologies at regional, urban and single-user scales. Energy 2019;182:254–68.
[24] Pappas SS, Ekonomou L, Karamousantas DC, Chatzarakis G, Katsikas S, Liatsis P. Electricity demand loads modeling using Auto Regressive Moving Average (ARMA) models. Energy 2008;33(9):1353–60.
[25] He C, Wu L, Liu T, Bie Z. Robust co-optimization planning of interdependent electricity and natural gas systems with a joint N-1 and probabilistic reliability criterion. IEEE Trans Power Syst 2018;33(2):2140–54.
[26] He C, Wu L, Liu T, Shahidehpour M. Robust co-optimization scheduling of electricity and natural gas systems via ADMM. IEEE Trans Sustain Energy 2017;8(2):658–70.
[27] A. J. Conejo, M. Carrión, and J. M. Morales, Decision making under uncertainty in electricity markets. New York: Springer; 2010.
[28] Shao C, Wang X, Shahidehpour M, Wang X, Wang B. An MILP-based optimal power flow in multicarrier energy systems. IEEE Trans Sustain Energy 2017;8(1):239–48.
[29] Lai X, Xie L, Xia Q, Zhong H, Kang C. Decentralized multi-area economic dispatch via dynamic multiplier-based Lagrangian relaxation. IEEE Trans Power Syst 2015;30(6):3225–33.
[30] Tang C, Xu J, Tan Y, Sun Y, Zhang B. Lagrangian relaxation with incremental proximal method for economic dispatch with large numbers of wind power scenarios. IEEE Trans Power Syst 2019;34(4):2685–95.

[31] Yu Y, Luh PB, Litvinov E, Zheng T, Zhao J, Zhao F, Schiro DA. Transmission contingency-constrained unit commitment with high penetration of renewables via interval optimization. IEEE Trans Power Syst 2017;32(2):1410–21.
[32] Farrokhifar M, Momayyezi F, Sadoogi N, Safari A. Real-time based approach for intelligent building energy management using dynamic price policies. Sustain Cities Soc. 2018;37:85–92.
[33] Fang J, Zeng Q, Ai X, Chen Z, Wen J. Dynamic optimal energy flow in the integrated natural gas and electrical power systems. IEEE Trans Sustain Energy 2018;9(1):188–98.
[34] Global wind atlas. https://globalwindatlas.info/area/Belgium. [Accessed 10 September 2018].
[35] Miao B, Chan SH. The economic feasibility study of a 100-MW Power-to-Gas plant. Int J Hydrogen Energy 2019;44(38):20978–86.
[36] Sun G, Chen S, Wei Z, Chen S. Multi-period integrated natural gas and electric power system probabilistic optimal power flow incorporating power-to-gas units. J Modern Power Syst Clean Energy 2017;5(3):412–23.
[37] Mingfei B, Jilai Y, Shahidehpour M, Yiyun Y. Integration of power-to-hydrogen in day-ahead security-constrained unit commitment with high wind penetration. J Modern Power Syst Clean Energy 2017;5(3):337–49.
[38] National renewable energy laboratory (NREL). https://www.nrel.gov/. [Accessed 10 September 2019].
[39] Lin Z, Chen H, Wu Q, Li W, Li M, Ji T. Mean-tracking model based stochastic economic dispatch for power systems with high penetration of wind power. Energy 2020;193:116–26.